تحليل التكثيف بالتماس المباشر على طبقة سائل مبرد مضطرب

عبد المحسن رجب و محمد باقر محسن المسلم

ملخص البحث

تناولت هذه الدراسة النظرية إنتقال الحرارة بالتكثيف بالتماس المباشر لبخار مشبع على جريان متوازي لطبقة سائل مبرد مضطرب. حيث تم تطوير النموذج النظري بحل معادلة الطاقة الحرارية مع الموازنة الحرارية لحالة جريان ثنائي الطور على سطح صلب معزول حرارياً. و لغرض حل المسألة الهندسية وظفت طريقة التقريب المتتابع . بينت الدراسة الحالية أن تأثير التخميد ، الناجم عن وجود سطح تلامس البخار – السائل، على اللزوجة الإضطرابية يعتمد على عدد رينولدز. وقد تم الحصول على علاقة ملائمة خلال تطوير نموذج إضطراب مناسب لإجراء الحسابات الهندسية للتكثيف بالتماس المباشر على الجريان المضطرب. و تبين النتائج ان عدد نسلت و سمك طبقة الجريان تعتمد على عدد رينولدز، جهد القص البيني، عدد برانتل، و عدد التبريد.

Introduction

Condensation heat transfer in direct contact mode can be encountered in a variety of industrial applications, such as nuclear industry (e.g. pressurizer under normal operating conditions, steam water interaction in safety analysis), chemical industry (e.g. mixing type heat exchangers, degassers, sea water desalting by multiple distillation) [1]. Renewed interest arises from energy transformation processes involving geothermal, solar and nuclear energy. Several types of direct contact condensers have been developed for energy conservation applications. Condensers of this type are employed because of their improved thermodynamic efficiency, trouble-free operation and smaller initial capital outlay besides the ability of mechanical design simplification and the possibilities to reduce the pressure drop in comparison with the conventional indirect heat transfer equipment. In this sense, packed type direct contact condensers have been proposed as an alternative efficient design for H_2S and CO_2 removal from geothermal steam before it enters the power generating turbines [2]. Film condensation phenomena had been analyzed first by Nusselt [3], who investigated the laminar film flow condensation along an infinite wall assuming no shear stress at the interface. After that many investigators have been studied film condensation. However, several investigators have studied condensation heat transfer in direct contact mode. There is few theoretical studies and a limited number of experimental studies that dealt with turbulent heat transfer in direct contact condensation owing to the difficulty of treating the vapor-liquid interface in a real or precise manner, whereas the experimental investigation is characterized by the difficulty of measuring the liquid film thickness due to the wavy interface. The complexity of the thermo-hydrodynamic coupling of the liquid and vapor phases has resulted in a large number of empirical correlations and some semi-theoretical correlations [4,5,6]. As a result, in many cases the attained solution is in fact an oversimplification for the problem. In an attempt to obtain a more precise model that may be applied to a wide range of Reynolds number, the present theoretical model is developed.

Analysis

Momentum Transfer

The flow system comprises turbulent liquid layer flows on an adiabatic

solid surface, with inlet mass flow rate of m_o and subcooled inlet temperature T_o. Saturated vapor with temperature T_s flows concurrently with the liquid layer and condenses on the liquid free surface as shown in Fig.1. The liquid flow is assumed to be steady and fully developed, and may be driven by interfacial shear stress, gravity, mean pressure gradient, or any combination of them. The vapor-liquid interface is taken undeformable and any waves are neglected. The physical properties of the liquid are assumed to be temperature independent.

Specification of the velocity profile and turbulence model is necessary for the formulation of the mathematical model. Fortunately, experimental turbulent velocity profile measurements that have been obtained from pipe-flow as well as from turbulent external boundary layer flow yield a logarithmic velocity profile in u^+, y^+ over a large part of the flow cross section, although approaching a linear relation immediately adjacent to the solid boundary. A two equations scheme (proposed by Prandtl and Tayler [7]) is used to describe the velocity distribution in the liquid layer. The complete velocity profile is then given by

$$u^+ = y^+$$

$$y^+ < 11.6 \qquad \ldots(1a)$$

$$u^* = 5.5 \ln y^+ + 2.5$$

$$11.6 \le y^+ \le \delta^* \qquad \ldots(1b)$$

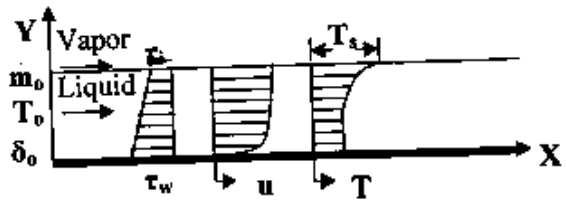

Fig.1 Direct contact condensation model.

Film Reynolds number is defined as

$$\mathrm{Re} = \frac{4\Gamma}{\mu} = 4\int_0^{\delta_o^+} u^+ . dy^+ = 4m_o^+ \qquad \ldots(2)$$

And the axial mass flow rate (m^+) is given by

$$m^+ = \int_0^{\delta^+} u^+ dy^+ \qquad \ldots(3)$$

Using relations (1a) and (1b) into the above equation and integrating, the axial film thickness can be written as

$$\delta^+ = \frac{m^+ + 54.29}{5.5(\ln \delta^+ - 1) + 2.5} \qquad \ldots(4)$$

Where

$$u^+ = u/u^* \;\; ; \;\; y^+ = y.u^*/\upsilon \;\; ;$$

$$\delta^+ = \delta.u^*/\upsilon \;\; ; \;\; m^+ = m/\mu.b \qquad \ldots(5)$$

Where (b) is the width of the solid surface.

Unfortunately, there is no suitable and ready turbulence model that can be applied directly to the present problem because of the presence of the vapor-liquid interface which requires a special way of manipulation. Such a way that depends on experimental data but keeps the theoretical insight should be proceeded. On the other hand, for developing such a turbulence model it is useful to inspect the near free-surface turbulence models that have been used to perform calculations of gas absorption into turbulent liquids since the feedback of the mass transfer on the interface motion is not significant in that case [8,9,10], consequently, one can expect that these models will be applicable to the condensation of a pure vapor, i.e., in the absence of noncondensable gases, for low surface shear stress. In this sense, Mills and Chung proposed a turbulence model that is suitable for film condensation for low vapor drag [10], it is the van Driest model, modified in the outer region of the film by the use of an eddy diffusivity

deduced from gas absorption measurements. The two models were terminated at their intersection. However, the application of Mills and Chung model to the present problem shows that it gives low Nusselt number values in general, although it is suitable for very low interfacial shear cases. As a result, this model is chosen to be developed in the present study in a way that provides a suitable turbulent viscosity profile for direct contact condensation on turbulent flow calculations for low and high interfacial shear as well. For the inner region of the liquid layer, the van Driest model of turbulence is modified by the inclusion of varying shear stress. For this purpose, distribution of shear stress at a distance y^+ from the solid boundary can be estimated by the balance of forces acting on a segment of the liquid. In dimensionless form, the shear stress distribution can be written as

$$\frac{\tau}{\tau_w} = 1 - (1 - \frac{\tau_i}{\tau_w})\frac{y^+}{\delta^+} \qquad \ldots(6)$$

The turbulent shear stress is defined as

$$\tau = (\mu + \rho.\varepsilon_m)\frac{du}{dy} \qquad \ldots(7)$$

or in dimensionless form

$$\frac{\tau}{\tau_w} = \left(1 + \frac{\varepsilon_m}{\nu}\right)\frac{du^+}{dy^+} \qquad \ldots(8)$$

Since diffusivity is much greater than molecular transport, the above relation can be written as

$$\frac{\tau}{\tau_w} = \left(\frac{\varepsilon_m}{\nu}\right)\frac{du^+}{dy^+} \qquad \ldots(9)$$

Based upon the mixing length concept the turbulent viscosity is defined as [13]

$$\varepsilon_m = l^2.\frac{du}{dy} \qquad \ldots(10)$$

the dimensionless form of this relation is

$$\frac{\varepsilon_m}{\nu} = l^{+2}.\frac{du^+}{dy^+} \qquad \ldots(11)$$

where,

$$l^+ = l.u^*/\upsilon \qquad \ldots(12)$$

Substitution of equation (11) into equation (9), and introducing the wall damping effect on the mixing length, the final relation of the turbulence mixing length with the wall damping effect and shear stress distribution is

$$l^+ = K.y^+\{1 - \exp(-y^+/26)\}.\sqrt{\tau/\tau_w} \qquad (13)$$

However much greater than the viscous stress the Reynolds stress is, the former being much larger at the wall than in laminar flow but becoming very small away from the wall, the later being large away from the wall and zero at the wall. Hence, the viscous one could be taken into account by substitution of equation (11) into equation (8), and this gives

$$\left(\frac{\varepsilon_m}{\nu}\right)^2 + \frac{\varepsilon_m}{\nu} - l^{+2}.\frac{\tau}{\tau_w} = 0 \qquad \ldots(14)$$

Equation (14) can be solved analytically, to yield finally the following relation

Since equation (15) begins to decrease beyond $y^+/\delta^+ \geq 0.6$, it is applied for $(0 \leq y^+/\delta^+ \leq 0.6)$. The outer region is divided into two sub-regions, in the first sub-region the diffusivity of the above equation is taken constant at its value at $y^+/\delta^+ = 0.6$, but only for $(0.6 \leq y^+/\delta^+ \leq yi^+/\delta^+)$ where yi^+ is the point at which the diffusivity is damped using the Mills and Chung near free surface diffusivity model [10],

$$\frac{\varepsilon_m}{\nu} = 6.47\times10^{-4}\,\frac{\rho.g^{1/3}.\nu^{4/3}.\mathrm{Re}^{1.678}}{\sigma.\delta^{+2/3}}\left(\delta^+ - y^+\right)^2 \qquad \ldots(16)$$

Henceforth, the eddy diffusivity profile in the outer region may be written as, for

$$0.6 \leq y^+/\delta^+ \leq yi^+/\delta^+$$

$$\frac{\varepsilon_m}{\nu}=\frac{1}{2}\left[-1+\sqrt{1+0.64\left\{0.6\delta^{+}\left[1-0.6\left(1-\frac{\tau_i}{\tau_w}\right)\right]\left(1-\exp\left(\frac{-0.6\delta^{+}}{26}\right)\right)\right\}^2}\right]$$

...(17)

and by equating equations (17) and (16) at $y^+= yi^+$, the eddy distribution for $yi^+/\delta^+ \le y^+/\delta^+ \le 1$ can be get as

$$\frac{\varepsilon_m}{\nu}=C\times 6.47\times 10^{-4}\,\frac{\rho g^{1/3}.\nu^{4/3}.\mathrm{Re}^{1.678}}{\sigma.\delta^{+2/3}}\left(\delta^{+}-y^{+}\right)^2 \qquad ...(18)$$

Where C is a constant resulting from equating the two above equations at $y^+= yi^+$.

yi^+ is the position at which interface-damping on the turbulent diffusivity is applied. Application of the developed turbulence model shows that as yi^+ increases, i.e., approaches the liquid-vapor interface, the resulted Nusselt number values substantially increases. This is attributable to the effect of the interface damping. While the effect of exerting no damping on the diffusivity at the free liquid surface shows very high values of Nusselt number. The comparison with the various available experimental data [1,12] using the present diffusivity profile shows that yi^+ depends on the Reynolds number. Consequently, the following relation for yi^+ is estimated

$$yi^+/\delta^+ = 0.81\,\mathrm{Re}^{0.018} \qquad ... (19)$$

Heat transfer

The heat balance equation for the system is

$$dm h_{fg}+dm c_p T_s+m c_p T_b=(m+dm)c_p(T_b+dT_b) \qquad ...(20)$$

Neglecting the minor value ($dm.c_p.dT_b$), equation (20) may be reshaped to permit integration as follows

$$d\{m[h_{fg}+c_p(T_s-T_b)]\}=0 \qquad ...(21)$$

and in dimensionless form becomes

$$d[m^+(1/S+T_b^+)]=0 \qquad ...(22)$$

with the boundary conditions in dimensionless form

$m^+ = m_o^+ = \mathrm{Re}/4;\ T_b^+ = 1$ at $x^+ = 0$ (23)

Where

$$T_b^+ = (T_s-T_b)/(T_s-T_o) \qquad ...(24)$$

Integration of equation (22) with the given boundary condition yields the following equation for the liquid film bulk temperature

$$T_b^+ = \frac{(\mathrm{Re}/4)(1+S)-m^+}{m^+.S} \qquad ...(25)$$

Since the value of m^+ is an unknown, the bulk temperature cannot be determined. Therefore another way to estimate it will be proceeded. Such a way depends on using the energy equation, with the earlier mentioned assumptions, could be written as

$$u(y)\frac{\partial T}{\partial x}=\frac{\partial}{\partial y}\left[(\alpha+\varepsilon_H)\frac{\partial T}{\partial y}\right] \qquad ...(26)$$

The statement that the fully developed temperature profile is invariant with x-direction can be expressed as [13]

$$\frac{\partial}{\partial x}\left(\frac{T_S-T}{T_S-T_b}\right)=0 \qquad ...(27)$$

Considering that the free stream steam temperature remains constant along the flow at the saturation temperature, T_s [12], and differentiating equation (27), gives

$$\frac{\partial T}{\partial x}=\left(\frac{T_S-T}{T_S-T_b}\right)\frac{dT_b}{dx} \qquad ...(28)$$

Using the above statement for $\partial T/\partial x$ into equation (26), in dimensionless form, this equation appears as

$$u^+\frac{T^+}{T_b^+}\cdot\frac{dT_b^+}{dx^+}=\frac{\partial}{\partial y^+}\left[\left(\frac{1}{\mathrm{Pr}}+\frac{\varepsilon_m/\nu}{\mathrm{Pr}_t}\right)\frac{\partial T^+}{\partial y^+}\right] \qquad (29)$$

with the conditions

$y^+=0 \quad \partial T^+/\partial y^+ = 0$ ...(30a)

$y^+=\delta^+ \quad T^+ = 0$ ...(30b)

Where

$x^+= x.u^*/\nu$ ...(31a)

$$T^+ = \frac{T_S - T}{T_S - T_o} \qquad \ldots(31b)$$

One way to solve equation (29) is by use of a successive approximation method because of the presence of T^+ in the left-hand side [13]. An approximate temperature profile, to be substituted for T^+ in the left-hand side of equation (29) can be obtained by imposing some simlification on the energy equation (26), and then it can be integrated twice with the boundary conditions given by equations (30a) and (30b), integration yields

$$T^+ = \int_{y^+}^{\delta^+} \frac{\int_0^{y^+} u^+ . T^+ \frac{1}{T_b^+}\left(-\frac{dT_b^+}{dx^+}\right) dy^+}{\left(\frac{1}{\mathrm{Pr}} + \frac{\varepsilon_m}{\nu . \mathrm{Pr}_t}\right)} dy^+ \qquad (32)$$

this position of analysis, the definition of the bulk temperature, T_b, which is given by

$$T_b^+ = \int_0^{\delta^+} u^+ T^+ dy^+ \Big/ \int_0^{\delta^+} u^+ dy^+ \qquad \ldots(33)$$

can be used to obtain the liquid layer mixed mean temperature. Using equation (32) into the previous equation gives

$$T_b^+ = \frac{\left(\frac{-1}{T_b^+} . \frac{dT_b^+}{dx^+}\right) \int_0^{\delta^+} \left[\int_{y^+}^{\delta^+} \frac{\int_0^{y^+} T^+ u^+ dy^+}{\left(\frac{1}{\mathrm{Pr}} + \frac{\varepsilon_m}{\nu . \mathrm{Pr}_t}\right)} dy^+ \right] u^+ dy^+}{\int_0^{\delta^+} u^+ dy^+}$$

$\ldots(34)$

The bulk temperature gradient(dT_b^+/dx^+) can be determined by differentiating equation (25),

$$\frac{dT_b^+}{dx^+} = \frac{-1}{m^+}\left(\frac{1}{S} + T_b^+\right)\frac{dm^+}{dx^+} \qquad \ldots(35)$$

and by substitution of T_b^+ from equation (25) into the above equation, the gradient of bulk temperature becomes

$$\frac{dT_b^+}{dx^+} = \frac{-\mathrm{Re}/4}{(m^+)^2}\left(\frac{1+S}{S}\right)\frac{dm^+}{dx^+} \qquad \ldots(36)$$

Substituting equation (36) into equation (34), and manpulating, the nondimensional

$$T_b^+ = \frac{\sqrt{\left(\frac{\mathrm{Re}/4}{m^{+2}} . \frac{(1+S)}{S} . \frac{dm^+}{dx^+}\right) \int_0^{\delta^+} \left[\int_{y^+}^{\delta^+} \frac{\int_0^{y^+} T^+ u^+ dy^+}{\left(\frac{1}{\mathrm{Pr}} + \frac{\varepsilon_m}{\nu . \mathrm{Pr}_t}\right)} dy^+ \right] u^+ dy^+}}{m^+}$$

$\ldots(37)$

Now equating equation (37) with equation (25) gives the dimensionless gradient of mass flow rate, which can be written as,

$$\frac{dm^+}{dx^+} = \frac{\left(\frac{m^+}{S}\right)\left\{(\mathrm{Re}/4)(1+S) - m^+\right\}/\sqrt{(\mathrm{Re}/4)(1+S)}\Big]^2}{\left\{\int_0^{\delta^+} \left[\int_{y^+}^{\delta^+} \frac{\int_0^{y^+} T^+ u^+ dy^+}{\left(\frac{1}{\mathrm{Pr}} + \frac{\varepsilon_m}{\nu . \mathrm{Pr}_t}\right)} dy^+ \right] u^+ dy^+ \right\}}$$

$\ldots(38)$

The value of m^+, and hence δ^+ and T_b^+ can be evaluated at any axial position (x^+) along the flow by solving equation (38) numerically. Where δ^+ can be evaluated using equation (4) by iteration.

The heat Transfer Coefficient

The local heat transfer coefficient can be obtained from heat balance (20) as

$$h_x = \frac{1}{b}\frac{h_{fg}}{(T_S - T_b)}\frac{dm}{dx} \qquad \ldots(39)$$

then the local Nusselt number is given by

$$Nu_x = \frac{\Pr.\delta_o^+}{S.T_b^+}.\frac{dm^+}{dx^+} \qquad \ldots(40)$$

Results and Discussions

Calculations of the liquid layer thickness, the wall and bulk temperaures and the local Nusselt numbers were carried out for various values of the condensation controlling parameters (Re, Pr, S, and τ_i/τ_w). For a better understanding of the influence of the related parameters on the condensation process, the results are plotted against the axial position, as shown in Figs. 2-12. The graph of the normalized thickness δ^+ against the axial distance x^+ is shown in Figs. 2-5. The observed increase in δ^+ with increment of x^+ is due to the continuous condensation at the liquid-vapour interface. Fig. 2 illustrates that the higher the Reynolds number the faster is the growth of δ^+ in the flow direction. This is attributable to the fact that the turbulent diffusivity increases significantly with the liquid flow rate increment, which leads to increase the condensation rate. Fig. 3 is drawn for different values of subcooling number, while the other control parameters (Re, Pr, and τ_i/τ_w) are kept constant. The higher values of S means higher rate of condensation, therefore thicker liquid film and higher rate of growth of the normalized thickness since S behaves as a potential of condensation. The influence of changes in the shear stress ratio τ_i/τ_w on the liquid layer thickness is illustrated in Fig.4. This figure indicates that The effect of variation of the shear stress ratio shows a significant increment in δ^+ with the increment of the shear ratio. This is due to the increased turbulent momentum diffusivity with the increment of the shear ratio, which increases the condensation rate. The less rate of growth of δ^+ at a distance far from the inlet is attributable to the fact that the higher the shear ratio the higher is the eddy heat diffusion in the liquid layer and the faster is the rate at which the liquid layer is heated up, which means a rapid increase in the liquid temperature in the flow direction as shown in Fig.6, in which the axial wall and mixed mean temperatures are plloted for low and high values of the shear parameter and subcooling number. This may lead to decrease the potential of condensation. The behaviour of δ^+ for different values of Prandtl number is shown in Fig.5. The values of δ^+ are proportional inversely to the values of Prandtl number, and the rate of growth of the values of δ^+ is slightly slower for low values of Prandtl number at an axial location far from the inlet. This is all attributable to the different distribution of the liquid layer resistance encountered at the various values of Prandtl number which affects the rate of the heat diffused through the liquid layer. This behavior may be explained with the aid of Fig.7, in which the values of the axial wall and bulk temperatures are drawn for low and high values of Reynolds and Prandtl numbers. In this figure, near the inlet of the flow, the lower the Prandtl number the higher is the response of the fluid to the penetration of heat through the liquid layer, which may mean higher condensation rate. Far from the inlet, all the other conditions being equal, the lower the Prandtl number the faster is the rate at which the liquid layer is heated up, which may lead to reduce the condensation potential. The opposite occurs for higher Prandtl numbers. This illustrates the relatively slower growth rates of δ^+ at a distance far from the inlet. Inspection of Figs. 2-5 shows that the effect of Pr on the condensation process is less than the effect of Re in the flow direction, and less than the significant effects of the shear stress parameter and S. This is attributed to the range of Prandtl number ($Pr > 1$) that is applicable in the present application, since the term (1/Pr) has less effect in comparison to the relative importance of the term of the turbulent eddy diffusion (ε_m/ν) in the energy equation.

Axial local Nusselt number was calculated and drawn in Figs. 8-11. Since Nusselt number is defined by ($h.\delta_o/k$),

therefore, its value depends on the value of ($h.\delta o$). While the initial film thickness δ_o depends on the inlet mass flow rate, which is reflected by Re, the heat transfer coefficient depends on the saturation temperature T_s, bulk temperature T_b, and the gradient of the condensate mass flow rate in the flow direction dm_c/dx, which are depend on the condensation controlling parameters. Although dm_c/dx generally decreases with the axial distance x^+ as it can be concluded from Figs.2-5; $(T_s - T_b)$ also decreases with x^+ as seen in Figs. 4 and 5. The behavior of (h) versus the axial distance (equation (39)) depends on the rate of decrease of these terms. However, Figs. 8-11 show the influence of the turbulence on the condensation heat transfer. The general trend visible in these figures is the increment of the Nusselt number along the axial distance x^+ for all the selected values of (Re, Pr, S, and τ_i/τ_w). This occurs due to the influence of the turbulence in the liquid layer which increases with increasing distance and mass flow rate in the flow direction, where the effect of the increased δ^+ due to the increasing mass flow along the flow has less influence than that of the turbulence. This may illustrate the importance of the appropriate treatment of the model of turbulence, since the estimated Nusselt number values depends mainly on the proper specification of this part of the problem. The variation of the local Nusselt number with the axial distance for various values of Re is shown in Fig. 8. This figure indicates that Nusselt number increases with the increment of Reynolds number. This means that the enhancement of the heat transfer due to the increased turbulence is more effective than the increased thermal resistance in the liquid, and hence, Nusselt number increases with the increment of Re. All of these contributions were reflected in the present developed turbulence distribution by the increased eddy diffusivity with the increment of Re, whereas $(\delta^+ - y_i^+)$, the distance to the free surface through which the turbulent diffusivity is damped, decreases with the increment of Re as illustrated by equation (19). This leads to decrease the thickness of the near-interface sublayers and hence the heat transfer is enhanced. In the light of the results of the influence of Pr on the axial local Nusselt number shown in Fig.9, it could be concluded that the heat transfer coefficient increases with the increment of Pr and so the Nusselt number. This may be attributed to that Nusselt number may be affected by the variation of the physical properties of the liquid caused by the variation of Pr. Fig. 10 indicates that the variation of the shear stress ratio shows a significant change in the Nusselt number. This occurs due to the increment of the interfacial shear stress, which enhances the convection and the turbulence in the liquid layer [12]. Fig. 11, in comparison with Figs.8-10, shows that Nusselt number is practically independent of the subcooling number S.

To prove the validity of the present theoretical analysis, the results obtained were compared with experimental data corresponding to cocurrent steam-water flow in a horizontal channel obtained by Lim et al. [12]. The comparison is made with the aid of other turbulence models [10,14] as presented in Fig. 12. This figure shows that the experimental results of the average Nusselt number Nu_{av} increase, decrease, or stay constant in the flow direction. This is attributable to the rates of decrease of the temperature difference $(T_s - T_b)$ and the gradient of the condensate with the increment of the axial distance. The average Nusselt number values (Nu_{av}) behave as illustrated and show this deviation from the theoretical results because for certain experimental conditions, the interface was smooth at the entrance and became wavy some distance downstream [12], and since the rates of change of these parameters are affected by the wavy nature of the interface. Nevertheless, this figure shows that the agreement between the theoretical and the experimental results is the best when the

present developed turbulence model is applied to the problem at the various liquid and steam Reynolds numbers.

Conclusions

The main points which can be drawn from the above analysis and discussion are

1. A theoretical model for direct contact condensation on turbulent subcooled liquid layer is developed and is able to predict the heat transfer characteristics without using the simplifications used by the previous investigators.
2. An appropriat turbulence model is developed to provide a satisfactory method for making engineering calculations of the process. It is found that the damping of the turbulent viscosity near the liquid-vapor interface depends mainly on Re and a suitable relation is found through this developmenmt.
3. The main controlling parameters on the condensation process on turbulent flow are Re, τ_i/τ_w, Pr, and S.
4. The thermal field is strongly affected by the variation of Re and τ_i/τ_w , wherease it is less influenced by Pr because (Pr > 1) in the present application. The effect of S can be ignored.
5. The influence of the condensation controlling parameters on δ^+ is characterised by the increase of δ^+ with the increment of the various parameters.
6. Nusselt number increases in general with the increment of any of the condensation controlling parameters. The effect of subcooling number on the heat transfer coefficient can be ignored.
7. The turbulence effects, which are increase by the increment of the mass flow rate and interfacial shear stress on both thermal and hydrodynamical fields are dominant along the flow.

References

1. Celata, G. P., Cumo, M., D'Annibale, F., Farello, G.E., and Focardi, G., "Theoretical and Experimental Study of Direct Contact Condensation on Water in Turbulent Flow", Experimental Heat Transfer, Vol. 2, pp. 129-148, (1989).
2. Karapantsios, T. D., and Karabelas, A. J., "Direct Contact Condensation in The Presence of Noncondensables over Free-Falling Films with Intermittent Liquid Feed", Int. J. Heat Mass Transfer, Vol. 38, No. 5, pp. 795-805,(1995).
3. Nusselt, W., "Die Oberflachenkondensation des Wasserdampfes" Zeitscriff Des Vereins Deutscher Inginuere, vol. 60, pp. 541-546, (1916).
4. Kim, J. H., and Bankoff, S. G., "Local Heat Transfer Coefficients for Condensation in Stratified Countercurrent Steam-Water Flows", Trans. of the ASME, Vol. 105, pp. 706-712, (1983).
5. Bankoff, S. G. and Kim, H. J., "Local Condensation Rates in Nearly Horizontal Stratified Countercurrent Flow of Steam and Cold Water", AICHE Symp. Ser. No. 225, Vol. 79, pp. 209-223, (1983).
6. Segev, A., and Collier, R. P., "A Mechanistic Model for Countercurrent Steam-Water Flow", Trans. of the ASME, Vol. 102, pp. 688-693, (1980).
7. Schlichting, H., "Boundary Layer Theory" , 4th ed., McGraw-Hill ,New York, pp. 489, (1960).
8. Bankoff, S. G., and Lee, S. C., "Condensation in Stratified Flow", Dataset No.16 Multiphase Science and Technology, Vol. 3, pp. 398-422, (1983).
9. Bankoff, S. G. "Some Condensation Studies Pertinent To LWR Safety", Int. J. Multiphase Flow, Vol. 6, pp. 51-67, (1980).
10. Mills, A. F., and, Chung, D. K., "Heat Transfer Across Turbulent Falling

Films", Int. J. Heat Mass Transfer, Vol. 16, pp. 694-696, (1973).
11. Ueda, H., Moller, R., Komori, S., and, Mizushima, T., "Eddy Diffusivity Near the Free Surface of Open Channel Flow", Int. J. Heat Mass Flow, Vol.20, pp. 1127-1136, (1977).
12. Lim, I. S., Tankin, R. S., and Yuen, M. C., "Condensation Measurement of Horizontal Cocurrent Steam-Water Flow", ASME J. Heat Transfer, Vol. 106, pp. 425-732, (1984).
13. Kays, W. M., and Crawford, M. E., "Convective Heat and Mass Transfer", McGraw -Hill Book Company, New York, (1983).
14. Limberg, H., "Warmeeaberang an Turbulent und Laminare Riselfilm", Int. J. Heat Mass Transfer, Vol. 16, pp. 1691-1702, (1973).

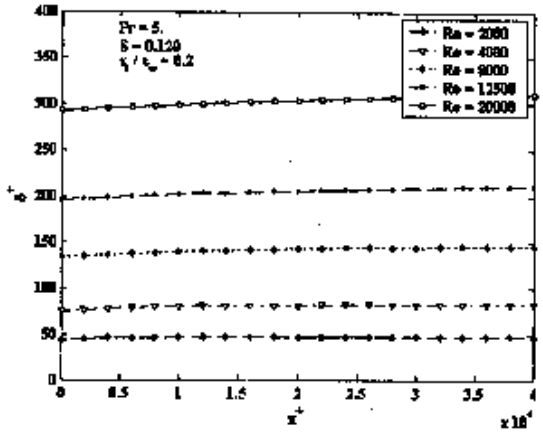

Fig.2 Dimensionless film thickness versus the axial distance for different values of Reynolds number.

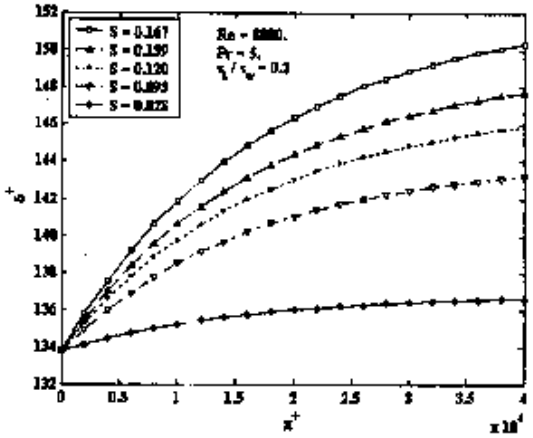

Fig.3 Dimensionless film thickness versus the axial distance for different values of subcooling number.

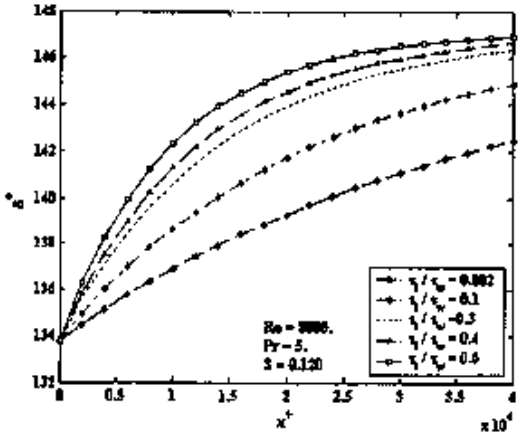

Fig.4 Dimensionless film thickness versus the axial distance for different values of shear stress ratio.

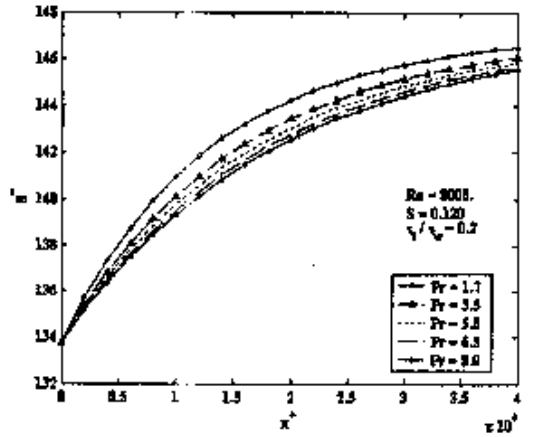

Fig.5 Dimensionless film thickness versus the axial distance for different values of Prandtl number.

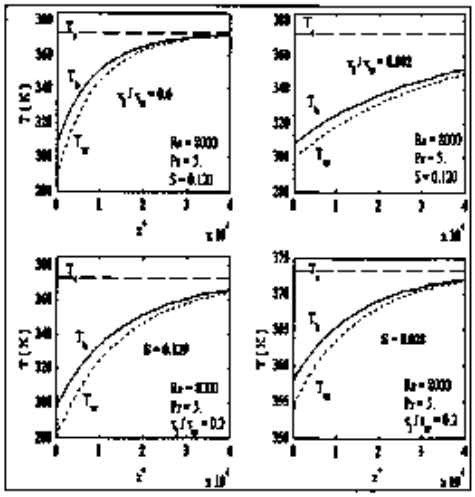

Fig.6 Axial wall and bulk temperatures for low and high values of shear stress ratio and subcooling number.

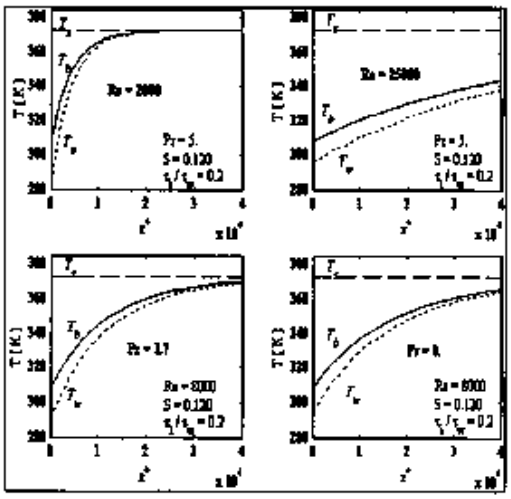

Fig.7 Axial wall and bulk temperatures for low and high values of Reynolds and Prandtl numbers.

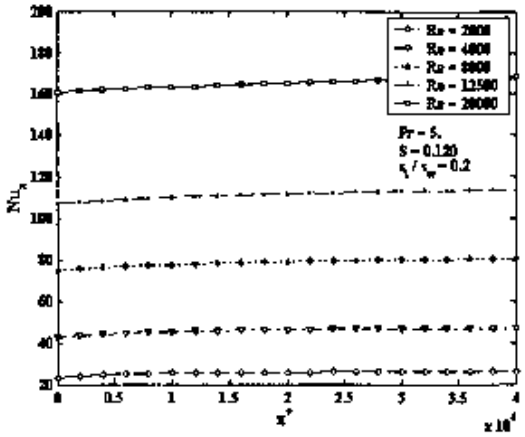

Fig.8 Axial local Nusselt number profiles as a function of Reynolds number.

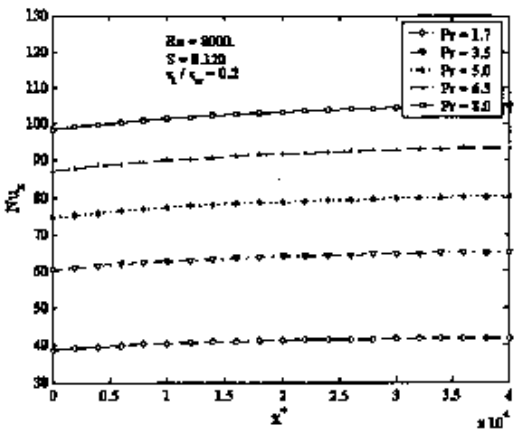

Fig.9 Axial local Nusselt number profiles as a function of Prandtl number.

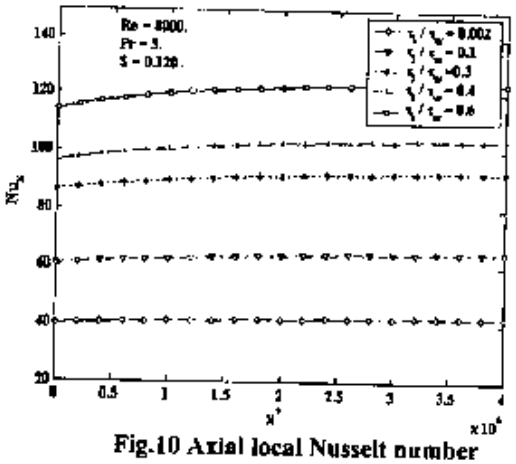

Fig.10 Axial local Nusselt number profiles as a function of shear stress ratio.

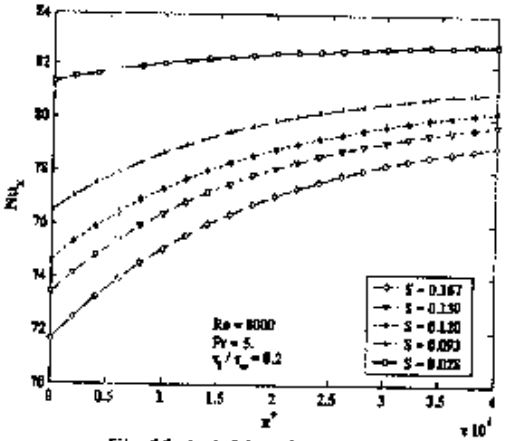

Fig.11 Axial local Nusselt number profiles as a function of subcooling number.

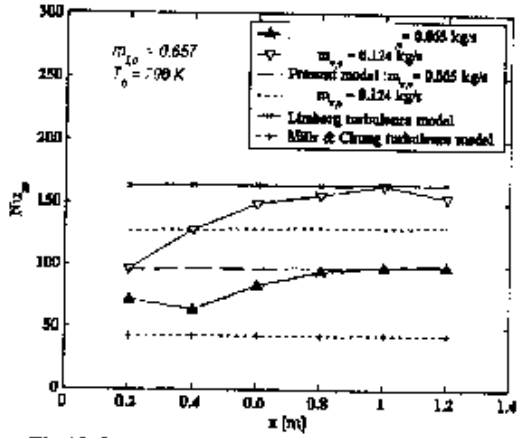

Fig.12 Comparison of the present theoretical results with experimental data of Lim et. al [7] for different values of inlet mass flow rate using other turbulence models.